

# 1 Evaluation and improvement of empirical models of global solar 2 irradiation: case study northern Spain

3 F. Antonanzas-Torres<sup>a,\*</sup>, A. Sanz-García<sup>a</sup>, F. J. Martínez-de-Pisón-Ascaibar<sup>a</sup>,  
4 O. Perpiñán-Lamigueiro<sup>b,c</sup>

5 <sup>a</sup>EDMANS Group, Department of Mechanical Engineering, University of La Rioja, Logroño, Spain.

6 <sup>b</sup>Electrical Engineering Department, EUITI-UPM, Ronda de Valencia 3, 28012 Madrid, Spain.

7 <sup>c</sup>Instituto de Energía Solar, Ciudad Universitaria s/n, Madrid, Spain

## 8 Abstract

9 This paper presents a new methodology to build parametric models to estimate global solar  
10 irradiation adjusted to specific on-site characteristics based on the evaluation of variable im-  
11 portance. Thus, those variables highly correlated to solar irradiation on a site are implemented  
12 in the model and therefore, different models might be proposed under different climates. This  
13 methodology is applied in a study case in La Rioja region (northern Spain). A new model is  
14 proposed and evaluated on stability and accuracy against a review of twenty-two already exist-  
15 ing parametric models based on temperatures and rainfall in seventeen meteorological stations  
16 in La Rioja. The methodology of model evaluation is based on bootstrapping, which leads to  
17 achieve a high level of confidence in model calibration and validation from short time series (in  
18 this case five years, from 2007 to 2011).

19 The model proposed improves the estimates of the other twenty-two models with average  
20 mean absolute error (MAE) of 2.195 MJ/m<sup>2</sup>day and average confidence interval width (95%  
21 C.I., n=100) of 0.261 MJ/m<sup>2</sup>day. 41.65% of the daily residuals in the case of SIAR and 20.12% in  
22 that of SOS Rioja fall within the uncertainty tolerance of the pyranometers of the two networks  
23 (10% and 5%, respectively). Relative differences between measured and estimated irradiation  
24 on an annual cumulative basis are below 4.82%. Thus, the proposed model might be useful  
25 to estimate annual sums of global solar irradiation, reaching insignificant differences between  
26 measurements from pyranometers.

27 *Keywords:* Solar global irradiation, empirical models, time series, evapotranspiration

## 28 Nomenclature

29 *BC* Bristow & Campbell model

30  $\Delta T$  Daily range of maximum and minimum temperatures

31  $\overline{\Delta T_c}$  Average  $\Delta T$  of the *calibration* dataset

32  $\Delta T_{i-1}$  Daily range of maximum and minimum temperatures on day *i-1*

33  $\Delta T_m$  Monthly average of  $\Delta T$

34  $\overline{\Delta T_t}$  Average  $\Delta T$  of the *testing* dataset

35 *h* Elevation above sea level

\*Corresponding author

Email address: antonanzas.fernando@gmail.com (F. Antonanzas-Torres)

- 36  $H$  Daily mean relative humidity
- 37  $J$  Julian day
- 38  $M$  Logical variable of rainfall
- 39  $MAE_{tes}$  Mean absolute error of testing
- 40  $MAE_{val}$  Mean absolute error of validation
- 41  $\overline{MAE_{val}}$  Average  $MAE_{val}$  for the whole set of stations
- 42  $n$  Length in days of the *validation* database
- 43  $P$  Rainfall
- 44  $P_c$  Yearly average rainfall in mm for the *calibration* dataset
- 45  $P_t$  Yearly rainfall in mm for the *testing* dataset
- 46  $p_{sat} [T_{max}]$  Vapor saturation pressure at  $T_{max}$
- 47  $R^2$  Coefficient of determination
- 48  $R_a$  Extraterrestrial irradiation
- 49  $R_{a,i-30}$  Extraterrestrial irradiation on day  $i-30$
- 50  $R_s$  Daily global solar irradiation
- 51  $\overline{R_s}$  Monthly mean of daily global irradiation
- 52  $\overline{R_{s,c}}$  Average  $R_s$  for the *calibration* period
- 53  $R_{s,est}$  Daily estimated irradiation
- 54  $R_{s,meas}$  Daily measured irradiation
- 55  $\overline{R_{s,t}}$  Average  $R_s$  for the *testing* period
- 56  $\overline{R_{MAE,val}}$  Average confidence interval width of MAE
- 57  $\overline{R_{RMSE,val}}$  Average confidence interval width of RMSE
- 58  $\overline{RMSE_{val}}$  Average  $RMSE_{val}$  for the whole set of stations
- 59  $RMSE_{tes}$  Root mean square error of testing
- 60  $T_{avg}$  Daily average air temperature
- 61  $T_{max}$  Daily maximum temperature
- 62  $T_{min}$  Daily minimum temperature
- 63  $\theta$  Julian angle
- 64  $W$  Daily mean wind speed

## 65 1. Introduction

66 Solar irradiation research is a field of rising interest due to its many applications, such as  
67 the study of evapotranspiration [1] and optimization of water demand in irrigation, crop fore-  
68 casting [2] from near-to-present measurements and estimates, the development and reduction  
69 of uncertainties in solar energy technologies (generation and internal rate of return) [3], the ad-  
70 justment of energy policies to promote solar energies, and research on climate change [4]. The  
71 high cost of measuring solar irradiation with pyranometers and the scarcity of long, reliable  
72 datasets for specific locations has propitiated the progress in estimators such as the analysis  
73 of satellite images [4, 5], artificial neural networks (ANN) [6, 7] and empirically-based para-  
74 metric models [8–10]; the latter estimating daily global horizontal irradiation ( $R_s$ ) from other  
75 meteorological variables.

76 Satellite-based  $R_s$  estimates are only provided with high resolution for specific areas in the  
77 planet, for example, 70S-70N, 70W-70E in the Satellite Application Facility for Climate Moni-  
78 toring (CM SAF) [11], Helioclim1 and Helioclim3 from SODA [12]. In other areas, resolution  
79 from satellite-based estimates is low, such as in some regions of South America and South-East  
80 Asia (INPE [13] and the National Renewable Energy Laboratory (NREL) [14] with 40x40km res-  
81 olution). The NASA Surface meteorology and Solar Energy (SSE) [15] coverage is global but  
82 resolution is very low ( $1^\circ \times 1^\circ$ ). Due to the effect of local microclimatic events on  $R_s$ , daily and an-  
83 nual divergence within a 40x40km or  $1^\circ \times 1^\circ$  cell might be significant [16]. In addition, satellite-  
84 based daily estimates are not generally freely accessible in the near present. For instance, the  
85 SODA provides  $R_s$  from Helioclim1 for the period 1985-2005, Helioclim3 for the year 2005 and  
86 from the SSE database for the period 1983-2005. These near-to-present estimates are necessary  
87 in different applications such as the estimation of evapotranspiration of previous days to fore-  
88 cast irrigation. As a result, the empirically-based parametric models stand out because of their  
89 high simplicity in estimating near-to-present  $R_s$  from measurements of commonly registered  
90 variables, generally registered with a higher distribution than the satellite resolution.

91 [17] and [18] developed the first parametric models to estimate  $R_s$  out of sunshine records  
92 and introduced the concept of the atmospheric transmittance that affects incoming extraterres-  
93 trial irradiation ( $R_a$ ). The common figure of most parametric models is that they account for  
94 latitude, solar declination, the Julian day ( $J$ ), and day length by including  $R_a$  [19]. [20] included  
95 mean daily cloud coverage to explain  $R_s$ . [21] introduced relative humidity and maximum tem-  
96 perature to estimate the monthly mean of the daily irradiation ( $\overline{R_s}$ ). However, the scarcity of  
97 sunshine and cloud cover records limits the usage of these methods to the location of validation.

98 [9], [22], and [8] developed the first models in which  $R_s$  is estimated through the daily range  
99 of maximum and minimum temperatures ( $\Delta T$ ). Note that in these models  $\Delta T$  behaves as an  
100 indicator of atmospheric transmittance, providing information about cloud cover. The higher  
101 emissivity of clouds than clear sky makes the maximum air temperature decrease and the min-  
102 imum temperature increase, and as a result the  $\Delta T$  decreases [23].

103 [24] studied the [9] model with  $\overline{R_s}$ , distinguishing between inland and coastal locations and  
104 obtaining higher accuracy in monthly than in daily estimates [25]. Other authors also modified  
105 the [9] model, introducing elevation [26], or modifying the square root by a Neperian logarithm  
106 [27] (the latter attributing it to [25]).

107 Rainfall ( $P$ ) was introduced as an explanatory variable directly [10, 28] or as a binary variable  
108 ( $M$ ) equal to 1 in days with some rainfall (denoted as rainy days) and 0 in days without any  
109 rainfall recorded (non-rainy days) [29–31]. According to previous papers, [30, 31] rejected using  
110  $\Delta T$  in his model, considering  $P$  sufficient to explain  $R_s$ . [30] also rejected  $R_a$  and applied Fourier  
111 series based on the julian angle ( $\theta$ ), corresponding to the angle in radians of the  $J$ .

112 [8] (hereinafter  $BC$ ) calculated  $\Delta T$  as the difference between the maximum temperature of

113 the day and the average of the minimum temperatures of the current day and the following  
 114 day. [32] modified the *BC* model, calculating  $\Delta T$  related to rainfall. [19] studied the influence  
 115 of  $\Delta T$  on estimations, calculated as the difference between the maximum ( $T_{max}$ ) and minimum  
 116 temperatures ( $T_{min}$ ) and as  $\Delta T$  as per *BC* and evaluated it with sixteen *BC* and [9] derived  
 117 models. Eventually, better estimations were achieved with  $\Delta T$  as the difference between  $T_{max}$   
 118 and  $T_{min}$ . The *BC* equation has also been modified by considering some parameters as constants  
 119 [1, 19, 33, 34]. The last of this papers attributed two new models to [33] and [35]. Additionally,  
 120 [33] concluded that [25] and *BC* models perform better for  $\bar{R}_s$  than for daily values. [36] and  
 121 latter [35] (who referred it as *BC*) included the monthly mean of the daily  $\Delta T$  to smooth the  
 122 results of the *BC* model. [36] also developed a model in which the daily average temperature  
 123 was introduced. [37, 38] also modified the *BC* model, introducing the  $R_a$  as a function of the  
 124 atmospheric transmittance. Indeed, several papers have proved the efficacy of the *BC* model by  
 125 comparing it with their own models or with other models, e.g. [1, 19, 23, 28, 29, 32–35, 39–42].

126 Most of parametric models to estimate  $R_s$  have been derived from the [9] and the *BC* models  
 127 by adding other variables that were proved to achieve better estimates where validated. How-  
 128 ever, a variable which might be correlated with  $R_s$  in a site, might not have such a dependency  
 129 in other site [26]. This paper proposes the evaluation of variable importance as a method to  
 130 adjust general models, i.e., the *BC* model. New models are then built by including important  
 131 variables, obtained by on-site specific relationships between predictors and  $R_s$ .

132 Several papers have already evaluated models according to test errors, assessing the capac-  
 133 ity of generalization under unproven data [23, 35, 39]. Nevertheless, models might generate  
 134 low test errors for a specific time series while still being unstable under slight variations in the  
 135 calibration data [43]. This paper also proposes an evaluation including stability and accuracy  
 136 under different initial conditions as model selection criteria, and implements it on twenty-four  
 137 parametric models (including two new models built on the method of evaluation of variable  
 138 importance) in seventeen meteorological stations in La Rioja (Spain). The estimates of the best  
 139 performing model are also compared with the CMSAF SIS satellite-derived database.

140 Table 1 summarizes the twenty-four models studied.

## 141 2. Meteorological data

142 The assessment is performed in La Rioja, a 5028 km<sup>2</sup> region of Spain with significant cli-  
 143 matic differences mainly due to differences in elevation and the smoothing influence of the  
 144 Ebro River. The daily meteorological data is provided by two public agencies, SOS Rioja [44]  
 145 and SIAR (Service of Agroclimatic Information of La Rioja) [45], with records taken every fifteen  
 146 and thirty minutes respectively.  $R_s$  is measured by SOS Rioja with *Geonica* sensors *CM-6B* and  
 147 *EQ08*, which are classed as First Class pyranometers according to the ISO9060 and by SIAR with  
 148 *Kipp&Zonen CM3* and *Hukseflux LP02*, which are Second Class pyranometers with 5% and 10%  
 149 daily tolerance levels respectively. The impact of the horizon effect on  $R_s$  has been analyzed and  
 150 not taken into account, since sky-view factors (ratio of visible sky related to the potential visible  
 151 sky) are between 0.985-0.999, substantially lower than the uncertainty of sensors and models  
 152 and therefore negligible.  $T_{max}$ ,  $T_{min}$  and  $P$  are recorded with tolerances of 0.1 °C and 0.1 mm by  
 153 SOS Rioja and 0.2 °C and 0.2 mm by SIAR. Additionally, average wind speed ( $W$ ) and relative  
 154 humidity ( $H$ ) are recorded with 0.3  $\frac{m}{s}$  and 3% tolerance respectively. Eventually, a total num-  
 155 ber of seventeen meteorological stations are selected (see Figure 1), with five complete years of  
 156 daily historical data on the aforesaid variables from 2007 to 2011. Spurious data are filtered out  
 157 according to the following limits,  $T_{max}$  lower than 45 °C,  $T_{min}$  higher than -20 °C, irradiance  
 158 lower than 1150  $\frac{W}{m^2}$ ,  $R_s$  lower than the daily  $R_a$ ,  $P$  lower than 40  $\frac{mm}{h}$ ,  $W$  lower than 30  $\frac{m}{s}$  and  $H$

159 lower than 100%. Spurious data account for less than 0.14% and are replaced by the average of  
 160 the previous and following measurements.

161 The time series of daily values from 2007 to 2011 of each station is divided into the *calibration*  
 162 dataset, running from 2007 to 2010 and the *testing* dataset, which covers 2011 alone. Table 2 pro-  
 163 vides general information about the main variables measured during the *calibration* and *testing*  
 164 periods.

165 Additionally,  $R_s$  from the CM SAF SIS for 2007-2011 is obtained to evaluate and compare er-  
 166 rors from the best-performing parametric model with those from this satellite-derived database.

### 167 3. Method

#### 168 3.1. Methodology of model evaluation

169 The analysis of robustness proposed leads to the stability of models being assessed under  
 170 many different initial conditions, and it is advisable to select the most suitable model, based  
 171 not only on the lowest testing errors [46]. The evaluation is based on bootstrapping to extract a  
 172 large amount of knowledge from a short time series [47, 48]. It is performed with each model at  
 173 each station. 80% of the *calibration* dataset for every station (1168 days) is sampled to calibrate  
 174 the parameters of each model. The remaining 20% (292 days) is used to validate the calibration  
 175 by calculating the validation mean absolute error ( $MAE_{val}$ ) and the validation root mean square  
 176 error ( $RMSE_{val}$ ). This process is repeated one hundred times, resampling the 80% of the *calibra-*  
 177 *tion* dataset and calculating  $MAE_{val}$  and  $RMSE_{val}$  to eventually obtain the confidence intervals  
 178 of the model parameters and errors.

$$MAE_{val} = \frac{1}{n} \sum_{i=1}^n |(R_{s,meas} - R_{s,est})| \quad (1)$$

$$RMSE_{val} = \sqrt{\frac{1}{n} \sum_{i=1}^n (R_{s,meas} - R_{s,est})^2} \quad (2)$$

179 Where,  $R_{s,meas}$  and  $R_{s,est}$  stand for daily measured irradiation and daily estimated irradiation  
 180 with the model to be validated.  $n$  stands for the length in days of the *validation* database (292  
 181 days).

182 Each model is calibrated with both spectral projected gradient methods for large-scale op-  
 183 timization [49] and a quasi-Newton algorithm known as the Broyden, Fletcher, Goldfarb and  
 184 Shanno (BFGS) method [50], which updates an approximation to the inverse Hessian along  
 185 with a point line search strategy [51]. The parameters calibrated minimize the sum of the square  
 186 residuals between the measurements ( $R_{s,meas}$ ) and the estimations ( $R_{s,est}$ ). A combination of  
 187 square errors in model calibration, and mean absolute errors ( $MAE$ ) is chosen as indicators of  
 188 model performance to reduce the impact of outliers in the evaluation [52].

189 The stability and accuracy of each model are assessed at the set of stations as a whole with  
 190 the mean confidence interval width of MAE ( $\overline{R_{MAE_{val}}}$ ) and the mean MAE ( $\overline{MAE_{val}}$ ). The un-  
 191 paired  $t - test$  is also evaluated to determine if  $MAE_{val}$  means are statistically different between  
 192 pairs of models within each station. The  $t$  is calculated with Equation 3 and then the  $p - value$   
 193 of the null hypothesis is derived.

$$t = \frac{\overline{x}_i - \overline{x}_j}{\sqrt{\frac{s_i^2 + s_j^2}{n}}} \quad (3)$$

194 where  $\overline{x}_i$  and  $\overline{x}_j$  are the mean  $MAE_{val}$  by bootstrapping with 100 samples of model  $i$  and  $j$ ,  $s_i$   
 195 and  $s_j$  the standard deviations and  $n$  the number of samples.

196 The capacity of generalization for non-common values is assessed with the confidence in-  
 197 terval width of RMSE ( $\bar{R}_{RMSE, val}$ ) and the mean RMSE ( $\overline{RMSE_{val}}$ ), as a result of the amplifying  
 198 property of this statistic with outliers.

199 The capability for generalization under unproven continuous data [53] is assessed within  
 200 the *testing* dataset with the testing MAE ( $MAE_{tes}$ ). The figures for the model parameters are  
 201 obtained from the median of the bootstrapping distributions.

202 The analysis described in this paper has been implemented using the free software envi-  
 203 ronment R [54] and several contributed packages: *gstat* [55] and *sp* [56] for the geostatistical  
 204 analysis, *optimx* [57] for the calibration of models, *solar* [58] for the solar geometry, *raster*  
 205 [59] for spatial data manipulation and analysis, and *rasterVis* [60] for spatial data visualiza-  
 206 tion methods.

### 207 3.2. Methodology of model development

208 The evaluation of variable importance leads to improve the performance of a general model  
 209 with specific relationships between predictors and outcomes of the site to be assessed. This  
 210 evaluation is performed by means of a *loess* smoother fit model, also known as locally weighted  
 211 polynomial regression, which is fitted between the outcome and the predictors [61]. Each point  
 212 ( $x$ ) of the dataset is fitted with a low-degree polynomial. The polynomial is adjusted with  
 213 weighted least squares, giving more weight to points near the point whose response is being  
 214 estimated and less weight to points further away. The weights are determined by their distance  
 215 from  $x$  with the tricubic weight function (Equation 3).

$$\omega(x) = (1 - |x^3|) \quad (4)$$

216 Eventually, the  $R^2$  is calculated for this model against the intercept only null model. The  $R^2$   
 217 is returned as a relative measure of variable importance.

218 The evaluation is performed with typically used variables such as  $P$ ,  $M$  and  $\Delta T$  and other  
 219 two non-commonly used variables  $W$  and  $H$  of the study day ( $i$ ) and of three days, two days  
 220 and the day before ( $i - 3, i - 2, i - 1$ ) and after ( $i + 3, i + 2, i + 1$ ). Those variables with high  $R^2$   
 221 are useful to improve the estimation of  $R_s$  within a classic model, such as the *BC*. As a result,  
 222 new *BC*-derived models are built according to Equations 5 & 6 with those important variables  
 223 and then evaluated according to Section 3.1.

$$R_s = a(1 - \exp(-b \cdot \Delta T^c)) R_a \cdot A + p_{n+1} \quad (5)$$

$$A = 1 + \sum_{j=1}^n p_j \cdot v_j \quad (6)$$

224 Where,  $A$  is the adjustment of the *BC* model according to the evaluation of variable impor-  
 225 tance,  $p$  is the parameter related to the variable  $v$  and  $n$  is the number of variables of adjustment.

## 226 4. Results and discussion

### 227 4.1. Model building

228 The evaluation of variable importance for La Rioja is collated in Table 3.  $\Delta T$ ,  $H$ , and  $M$   
 229 show values of  $R^2$  higher than 0.15. Throughout the analysis of variable importance it might  
 230 be proved that rainfall in this region should be explained with  $M$  instead of  $P$  (0.153 vs. 0.056),  
 231 which however, is implemented in models 6 and 7. As a result,  $P$  is rejected as a variable

232 to explain  $R_s$ . Equation 6 might be fitted with different combinations of variables ( $p_j$ ) and  
 233 therefore, different models might be built and then evaluated as per Section 3.1. Two different  
 234 sets of models are built regarding inputs used. The first set of models, constituted by 9 models,  
 235 is built considering commonly registered meteorological variables ( $T_{max}$ ,  $T_{min}$  and  $M$ ). The  
 236 second set of models also integrates  $W$  and  $H$  and is composed by 3 different models. Since  
 237  $\Delta T$  is already considered within the  $BC$  model, only  $\Delta T_{j \neq 1}$  are considered in  $A$ . Eventually,  
 238 only  $p_j$  and  $p_{j \pm 1}$  are relevant in  $R_s$ , showing lower errors in the evaluation.  $M_j$ ,  $M_{j \pm 1}$ ,  $\Delta T_j$  and  
 239  $\Delta T_{j \pm 1}$  provide information about the cloud coverage [23] and  $W$  and  $H$  refine the sky clearness.  
 240 However,  $H_{j \neq 1}$  and  $W_{j \neq 1}$  reduce the robustness of models and increase errors.  $M$ ,  $M_{i-1}$  and  
 241  $M_{i+1}$  were already implemented in the [29] models (models 18 and 19). Equations 6 and 7 show  
 242 the final models proposed for both afore-mentioned sets.

$$R_s = R_a \cdot a (1 - \exp(-b \cdot \Delta T^c)) \cdot (1 + d \cdot M_{j-1} + e \cdot M_j + f \cdot M_{j+1} + g \cdot \Delta T_{j+1} + h \cdot \Delta T_{j-1}) + l \quad (7)$$

$$R_s = R_a \cdot a (1 - \exp(-b \cdot \Delta T^c)) \cdot (1 + d \cdot M_{j-1} + e \cdot M_j + f \cdot M_{j+1} + g \cdot \Delta T_{j+1} + h \cdot \Delta T_{j-1} + l \cdot W_j + m \cdot H_j) + n \quad (8)$$

#### 243 4.2. Evaluation of parametric models

244 The results of the robustness assessment are collated in Figure 2, showing the 95% confi-  
 245 dence intervals (95% C.I., n=100) of the  $MAE_{val}$  obtained by bootstrapping and also the test  
 246 errors ( $MAE_{tes}$ ). Narrow confidence intervals and low values of  $MAE_{val}$  imply both stability  
 247 and accuracy in models, and low  $MAE_{tes}$  means high capacity for generalization within the  
 248 *testing* period. Several models, such as 12 and 13 at station 1, 12-14 at station 8, 10 and 12 at  
 249 the station 12, and 1-5, 7-10, 12 and 20 at the station 17 among others, generate wide confi-  
 250 dence intervals and high values of  $MAE_{val}$  and at the same time low  $MAE_{tes}$ . In spite of the  
 251 high capacity for generalization of the afore-mentioned models within the *testing* period, the  
 252 methodology proposed leads to their selection being avoided. For instance, stable and accurate  
 253 models such as 24 should be selected at station 17 instead of model 20, although the latter gener-  
 254 erates lower  $MAE_{tes}$ . The robustness assessment is found useful when only short and biased  
 255 time series are available to evaluate models.

256 The stability of models is assessed through the  $\overline{R_{MAE, val}}$  of the model for the whole set of  
 257 stations (Table 4). The proposed models (models 23 and 24) improve the results of [29] (models  
 258 18 and 19) with  $\overline{R_{MAE, val}}$  of 0.360 and 0.261 MJ/m<sup>2</sup>day and 0.387 and 0.385 MJ/m<sup>2</sup>day, respec-  
 259 tively. Therefore, model 23 is considered the most stable for this region by means of rainfall and  
 260 daily range of temperatures. However, a significant improvement in stability is achieved intro-  
 261 ducing  $W$  and  $H$  in addition to  $\Delta T$  and  $M$ , as seen with model 24. Models 1-10, 15, 20 and 22  
 262 generate similar  $\overline{R_{MAE, val}}$  between [0.42-0.45] MJ/m<sup>2</sup>day, and models 12-14, 17 and 21 between  
 263 [0.48-0.53] MJ/m<sup>2</sup>day. The low stability of models 11 and 16, with  $\overline{R_{MAE, val}}$  of 0.761 and 0.764  
 264 MJ/m<sup>2</sup>day, might be explained by the inclusion of  $R_{a, i-30}$  and the lack of  $R_a$ , respectively.

265 Model accuracy is assessed via the average of  $MAE_{val}$  for the whole set of stations ( $\overline{MAE_{val}}$ ).  
 266 The highest accuracy in predictions is also achieved with models 24, 23 and 18 with  $\overline{MAE_{val}}$  of  
 267 2.195, 2.247 and 2.317 MJ/m<sup>2</sup>day (Table 4). In addition, model 23 and 24 obtain the lowest  
 268 values of  $MAE_{val}$  of  $1.886 \pm 0.161$  and  $1.887 \pm 0.090$  (95% C.I., n=100) MJ/m<sup>2</sup>day (Figure 2)  
 269 at station 11 (*Calahorra*). According to the  $t - test$  the  $MAE_{val}$  mean is statistically lower in  
 270 model 24 than any other model in all stations, except in station 9, in which models 18, 19 and  
 271 23 have lower  $MAE_{val}$  mean (Table 5). From this test, it can also be deduced that model 23 has  
 272 statistically lower  $MAE_{val}$  than models 18 and 19 in all stations.

273 The original *BC* model (model 8) achieves lower  $\overline{MAE_{val}}$  (2.617 MJ/m<sup>2</sup>day) than other *BC*-  
 274 derived models such as 10-14 and 20-21. Models 3, 5 and 6, derived from [9] (model 1), obtain  
 275 lower  $\overline{MAE_{val}}$  than the initial model. [10] (model 7), derived from [22] (model 15) improves  
 276 the  $\overline{MAE_{val}}$  from 2.719 MJ/m<sup>2</sup>day (model 15) to 2.534 MJ/m<sup>2</sup>day (model 7). [30] and [31]  
 277 models (models 16 and 17), in which  $\Delta T$  is not considered, achieve  $\overline{MAE_{val}}$  of 6.315 MJ/m<sup>2</sup>day  
 278 and 3.405 MJ/m<sup>2</sup>day. [38] (model 11) generates a  $\overline{MAE_{val}}$  of 4.426 MJ/m<sup>2</sup>day, due to its high  
 279 dependency on the  $R_{a,i-30}$ .

280 The capacity of generalization of models to non-common days is assessed through the  $\overline{RMSE_{val}}$   
 281 and  $\overline{R_{RMSE, val}}$  in Table 4. The model proposed (model 24) behaves with lower  $\overline{RMSE_{val}}$  (2.879  
 282 MJ/m<sup>2</sup>day) than the other models analyzed and also with a lower  $\overline{R_{RMSE, val}}$  (0.361 MJ/m<sup>2</sup>day).  
 283 This model generates lower median of  $\overline{RMSE_{val}}$  in all stations, except in station 9, in which is  
 284 lower in models 18, 19 and 23.

285 Eventually, the models 24 (model proposed by means of  $\Delta T$ ,  $M$ ,  $W$  and  $H$ ) and model 23  
 286 (model proposed by means of  $\Delta T$  and  $M$ ) are considered the most suitable models for estimat-  
 287 ing  $R_s$  in La Rioja. Notwithstanding, the model evaluation is focused on model 24 due to its  
 288 superior stability and accuracy. 41.65% of the daily residuals in the case of SIAR and 20.12% in  
 289 that of SOS Rioja fall within the uncertainty tolerance of the pyranometers of the two networks  
 290 (10% and 5%, respectively). However, smaller differences between  $R_{s, meas}$  and  $R_{s, est}$  are found  
 291 in Figure 4 when considering yearly sums of  $R_s$ . Yearly sums of  $R_s$  fall within the uncertainty  
 292 tolerance of the pyranometers in all estations during the five years (2007-2011) with a higher  
 293 divergence of 4.823% in 2011. Regarding the relative differences between measured and esti-  
 294 mated monthly sums of  $R_s$  in 2011, 91.7% and 45.8% of the cases in SIAR and SOS Rioja stand  
 295 within the tolerance of pyranometers.

296 The performance of the whole set of models is related to elevation, as shown in Figure 5,  
 297 with higher  $\overline{MAE_{val}}$  being produced at higher altitudes, as evidenced at stations over 1000  
 298 m. A suitable explanation of this behaviour might be because there is more meteorological  
 299 variability in the mountainous areas of La Rioja, than in the lowlands [26]. A slight correlation  
 300 with elevation is found in models 10, 14 18-20, 23 and 24, not as marked as with other models.

301 Figure 6 shows the parameters calibrated on model 24 to estimate  $R_s$  in  $Wh/m^2 day$ . High  
 302 variability between stations is found within the non explanatory constant (parameter  $n$ ). This  
 303 variability was also reported by [29] and might be explained by the strong site dependency de-  
 304 scribed by [26, 62]. [23] and [19] described correlations between the parameters and the distance  
 305 between stations or latitude and longitude. Nevertheless, no correlation between the values of  
 306 the parameters and latitude, longitude, elevation or distance between stations is found in model  
 307 24.

308 The effect of rain in model 24 is shown in Figure 7, in which the MAE of non-rainy days  
 309 is on average 11.3% lower than that of rainy days for the whole set of stations. This is also  
 310 widely found in the rest of the models, and is explained by the fact that solar irradiation is more  
 311 complex on rainy and overcast days [10]. 2011 was an especially dry year in La Rioja, with 19.7%  
 312 less rainfall than the average for the *calibration* period 2007-2010 (Table 2), so the  $\overline{MAE_{tes}}$  figures  
 313 are significantly low in comparison with the confidence intervals of the  $\overline{MAE_{val}}$  in Figure 2.  
 314 However, this tendency is broken with some models at station 14 (*Moncalvillo*), where the  
 315  $\overline{MAE_{tes}}$  are higher than the  $\overline{MAE_{val}}$ . More cloud cover in the *testing* period, evidenced by  $\overline{\Delta T_t}$   
 316 being lower than the  $\overline{\Delta T_c}$  seen in Table 2 at station 18, might explain this finding [23].

### 317 4.3. Evaluation compared with CM SAF

318 The mean MAE registered by CM SAF related to  $R_{s, meas}$  is 1.983 MJ/m<sup>2</sup>day with a standard  
 319 deviation of 0.517 MJ/m<sup>2</sup>day, in average 10.7% lower than  $\overline{MAE_{val}}$  from model 24, although  
 320 in stations 9, 11, 14, 16 and 17  $\overline{MAE_{CMSAF}}$  is higher than the confidence interval (95% C.I.,



321 n=100). The  $RMSE_{CMSAF}$  is 3.207 MJ/m<sup>2</sup>day with a standard deviation of 0.449 MJ/m<sup>2</sup>day,  
 322 being higher than the confidence interval (95% C.I., n=100) in stations 6, 7, 9, 12, 14, 16 and 17.  
 323 Table 6 shows the errors of testing (testing dataset) for the model 24 and CM SAF. It might be  
 324 deduced that CM SAF generally performs with lower errors than model 24 except in stations  
 325 9, 11, 14, 16 and 17 (same stations with lower  $MAE_{val}$  and  $RMSE_{val}$  than CM SAF), in which  
 326 model 24 is superior.

327 Figure 3 shows the performance of model 24 with new data from the testing database. This  
 328 model achieves coefficients of determination ( $R^2$ ) with linear regression of [0.87-0.91] and [0.79-  
 329 0.87] for stations below and above 1000 m respectively. The coefficients of determination from  
 330 CM SAF against  $R_{s,meas}$  ( $R^2_{CMSAF}$ ) are significantly higher than  $R^2$ , but also showing a relation  
 331 with elevation, being lower at higher elevation.

332 The annual irradiation estimated by CM SAF is significantly higher than the  $R_{s,meas}$ , which  
 333 was also found in Spain by [63]. Stations 11, 14, 16 and 17 present relative differences substan-  
 334 tially above the tolerance of pyranometers reaching 22.95% in station 14 in year 2011. Thus, the  
 335 model proposed (model 24) is able to estimate more accurately annual irradiation in this region  
 336 than the CM SAF during years 2007-2011.

337 It could be argued that, because the CM SAF estimations show higher  $R^2$  values, their worse  
 338 results in the RMSE and MAE indicators may be improved with a local calibration. This ap-  
 339 proach was developed in [63] with a geostatistical interpolation (kriging with external drift) us-  
 340 ing data from a network of 301 ground stations and also CM SAF. A more simplified approach  
 341 is to use a parametric model as Equation 9,

$$R_s = R_a \cdot \left( a \cdot \frac{R_{s,cmsaf}}{R_a} + b \right) \quad (9)$$

342 where the CMSAF estimations are normalized with the extraterrestrial radiation and cali-  
 343 brated with the on-ground radiation measurements. This approach has been analyzed achiev-  
 344 ing  $\overline{MAE_{val}}$  and  $\overline{RMSE_{val}}$  of 1.913 and 2.987 MJ/m<sup>2</sup>day with  $\overline{R_{MAE,val}}$  and  $\overline{R_{RMSE,val}}$  of 0.422  
 345 and 0.886 MJ/m<sup>2</sup>day, respectively. The  $R^2$  in this parametrization is also lowered respect the  
 346 actual  $R^2$  of CM SAF. This means that it is only improved the  $\overline{MAE_{val}}$  respect to the model 24  
 347 while getting the other indicators worse. However, this re-calibration of CM SAF leads to lower  
 348 errors in annual sums of global irradiation with CM SAF (in 15 stations the error is within the  
 349 5% and a 5.7% maximum error). The Table 7 shows parameters of Equation 9, where  $a_{mean}$ ,  
 350  $b_{mean}$ ,  $a_{sd}$ ,  $b_{sd}$  are the average and standard deviations of  $a$  and  $b$ .

## 351 5. Conclusions

352 The methodology proposed of model development of adjusting a general model with the on-  
 353 site peculiarities based on the evaluation of variable importance is proved appropriated within  
 354 the case study of La Rioja region (northern Spain). The high site dependency of  $R_s$  related to  
 355 the meteorological trends suggests the adjustment of general parametric models (such as the  
 356 BC and [9] models) with those variables that show higher correlation with  $R_s$ . By means of this  
 357 methodology, different models might be proposed in locations with different climates. The new  
 358 model includes  $M$ ,  $M_{i-1}$ ,  $M_{i+1}$ ,  $\Delta T_{i-1}$ ,  $\Delta T_{i+1}$ ,  $W$ ,  $H$  as explanatory variables (derived from the  
 359 evaluation of variable importance) that adjust the BC model in La Rioja.

360 The methodology proposed of model evaluation is based on bootstrapping and proves use-  
 361 ful in selecting models according to stability and accuracy and not only based on test errors. The  
 362 proposed model is evaluated with this methodology against a review of twenty-two already ex-  
 363 isting parametric models at seventeen meteorological stations within La Rioja. The new model  
 364 improves the estimates of the other twenty-two models with  $\overline{MAE_{val}}$  of 2.195 MJ/m<sup>2</sup>day and

365  $\overline{R_{MAE, val}}$  of 0.261 MJ/m<sup>2</sup>day. However, several BC derived models (10-14, 20-21) fail to improve  
366 the estimates of the original model. This might be explained because these models include vari-  
367 ables that do not show high correlation with  $R_s$  (such as  $P$ ) within La Rioja. In addition, sig-  
368 nificant differences in stability between models and meteorological stations are recorded with  
369 these models. The performance of the model proposed is compared with  $R_{s, CMSAF}$ , obtaining  
370 lower confidence interval (95% C.I., n=100) of  $MAE_{val}$  than  $MAE_{CMSAF}$  in 5 stations and for  
371  $RMSE_{val}$  in 7 stations.

372 Rainfall and elevation are shown to influence the accuracy of model performance (gener-  
373 ating higher errors in rainy days and also at higher stations). The fact that the *testing* dataset  
374 (year 2011) was significantly drier than the *calibration* dataset (years 2007-2010) explains the low  
375  $MAE_{tes}$  recorded.

376 The residuals of estimates are found to have yearly periodicity, with higher relative residuals  
377 when meteorological variability is greater. 41.65% of the daily residuals in the case of SIAR and  
378 20.12% in that of SOS Rioja fall within the uncertainty tolerance of the pyranometers of the two  
379 networks (10% and 5%, respectively). However, the annual relative differences between  $R_{s, meas}$   
380 and  $R_{s, est}$  are lower than 4.82%, which means that estimates are within the confidence interval  
381 of pyranometers.

382 The analysis of parametric models against the CM SAF satellite-derived irradiation data  
383 shows that the mean  $MAE_{CMSAF}$  is in average 10.7% lower than  $\overline{MAE_{val}}$ , but also that in 5 sta-  
384 tions the  $\overline{MAE_{val}}$  is significantly lower than the one of CM SAF. This tendency is also common  
385 with the  $RMSE$ , which is generally lower with CM SAF, but not always (7 stations). Never-  
386 theless, attending to the annual irradiation it has been proved that the model proposed (model  
387 24) achieves significantly better estimates than the CM SAF, which over-estimates solar irradi-  
388 ation within the region studied. The possibility of shades on the positions of stations over the  
389 CM SAF estimates has been previously analyzed and rejected. As a result, the proposed model  
390 might be useful to estimate annual sums of  $R_s$ , reaching insignificant differences with  $R_s$  from  
391 pyranometers and also to be used on a daily basis when correctly calibrated with on-ground  
392 data.

### 393 Acknowledgements

394 We are indebted to the University of La Rioja (fellowship FPI 2012) and the Research Institute  
395 of La Rioja (*IER*) for funding parts of this research.

### 396 References

- 397 [1] Running, S. W., Nemani, R. R., Hungerford, R. D., 1987. Extrapolation of synoptic meteo-  
398 rological data in mountainous terrain and its use for simulating forest evapotranspiration  
399 and photosynthesis. *Can. J. For. Res.* 17, 472–483.
- 400 [2] Crop Growth Monitoring System  
401 URL [http://www.marsop.info/marsopdoc/cgms92/2\\_2\\_2\\_en.htm](http://www.marsop.info/marsopdoc/cgms92/2_2_2_en.htm)
- 402 [3] Beyer, H. G., Polo-Martinez, J., Suri, M., Torres, J. L., Lorenz, E., Muller, S. C., Hoyer-Klick,  
403 C., Ineichen, P., 2009. Mesor: Management and exploitation of solar resource knowledge.  
404 D 1.1.3 Report on Benchmarking of Radiation Products., 1–160.
- 405 [4] Schulz, J., Albert, P., Behr, H.-D., Caprion, D., Deneke, H., Dewitte, S., Dürr, B., Fuchs, P.,  
406 Gratzki, A., Hechler, P., Hollmann, R., Johnston, S., Karlsson, K.-G., Manninen, T., Müller,  
407 R., Reuter, M., Riihelä, A., Roebeling, R., Selbach, N., Tetzlaff, A., Thomas, W., Werscheck,

- 408 M., Wolters, E., Zelenka, A., 2009. Operational climate monitoring from space: the EUMET-  
409 SAT satellite application facility on climate monitoring (CM-SAF). *Atmos. Chem. Phys.*  
410 9 (5), 1687–1709.
- 411 [5] Posselt, R., Mueller, R., Stockli, R., Trentmann, J., 2012. Remote sensing of solar surface ra-  
412 diation for climate monitoring - the CM-SAF retrieval in international comparison. *Remote*  
413 *Sens. Environ.* 118 (0), 186 – 198.
- 414 [6] Rahimikhoob, A., 2010. Estimating global solar radiation using artificial neural network  
415 and air temperature data in a semi-arid environment. *Renew. Energ.* 35 (9), 2131 – 2135.
- 416 [7] Senkal, O., 2010. Modeling of solar radiation using remote sensing and artificial neural  
417 network in Turkey. *Energy* 35 (12), 4795 – 4801.
- 418 [8] Bristow, K. L., Campbell, G. S., 1984. On the relationship between incoming solar radiation  
419 and daily maximum and minimum temperature. *Agric. For. Meteorol.* 31 (2), 159 – 166.
- 420 [9] Hargreaves, G. H., 1981. Responding to tropical climates. In: 1980-81 Food and Climate  
421 Review. The Food and Climate Forum. Aspen Institute for Humanistic Studies, Boulder,  
422 Colorado, pp. 29–32.
- 423 [10] Jong, R. D., Stewart, D. W., 1993. Estimating global solar radiation from common meteorolo-  
424 gical observations in western Canada. *Can. J. Plant Sci.* 73 (2), 509–518.
- 425 [11] The Satellite Application Facility on Climate Monitoring (CM SAF)  
426 URL <http://www.cmsaf.eu>
- 427 [12] SODA  
428 URL <http://www.soda-is.com/eng/index.html>
- 429 [13] INPE  
430 URL <http://www.inpe.br>
- 431 [14] National and Renewable Energy Laboratory (NREL)  
432 URL <http://www.nrel.gov/gis/solar.html>
- 433 [15] NASA Surface meteorology and Solar Energy (SSE)  
434 URL <http://maps.nrel.gov/SWERA>
- 435 [16] Perez, R., Seals, R., Stewart, R., Zelenka, A., Estrada-Cajigal, V., 1994. Using satellite-  
436 derived insolation data for the site/time specific simulation of solar energy systems. *Solar*  
437 *Energy* 53 (6), 491-495.
- 438 [17] Angstrom, A., 1924. Solar and terrestrial radiation. Report to the international commission  
439 for solar research on actinometric investigations of solar and atmospheric radiation. *Q. J.*  
440 *Roy. Meteor. Soc.* 50 (210), 121–126.
- 441 [18] Prescott, J., 1940. Evaporation from a water surface in relation to solar radiation. *Trans. R.*  
442 *Soc. So. Augst.* 64, 114–125.
- 443 [19] Liu, X., Mei, X., Li, Y., Wang, Q., Jensen, J. R., Zhang, Y., Porter, J. R., 2009. Evaluation of  
444 temperature-based global solar radiation models in China. *Agric. For. Meteorol.* 149 (9),  
445 1433 – 1446.

- 446 [20] Supit, I., van Kappel, R., 1998. A simple method to estimate global radiation. *Sol. Energy*  
447 63 (3), 147 – 160.
- 448 [21] Ododo, J., 1997. Prediction of solar radiation using only maximum temperature and rela-  
449 tive humidity: south-east and north-east Nigeria. *Energy Convers. Manage.* 38 (18), 1807 –  
450 1814.
- 451 [22] Richardson, C. W., 1981. Stochastic simulation of daily precipitation, temperature, and so-  
452 lar radiation. *Water Resour. Res.* 17 (1), 182–190.
- 453 [23] Trnka, M., Zalud, Z., Eitzinger, J., Dubrovsky, M., 2005. Global solar radiation in Cen-  
454 tral European lowlands estimated by various empirical formulae. *Agric. For. Meteorol.*  
455 131 (12), 54 – 76.
- 456 [24] Allen, R. G., 1995. Evaluation of procedures for estimating mean monthly solar radiation  
457 from air temperature. Report. Food and Agricultural Organization of the United Nations  
458 (FAO), Rome., Rome.
- 459 [25] Allen, R. G., 1997. Self-calibrating method for estimating solar radiation from air tempera-  
460 ture. *J. Hydrol. Eng.* 2 (2), 56–67.
- 461 [26] Annandale, J. G., Jovanovic, N. Z., Benade, N., Allen, R. G., Mar. 2002. Software for missing  
462 data error analysis of Penman-Monteith reference evapotranspiration. *Irrig. Sci.* 21 (2), 57 -  
463 67.
- 464 [27] Chen, R., Ersi, K., Yang, J., Lu, S., Zhao, W., 2004. Validation of five global radiation models  
465 with measured daily data in China. *Energy Convers. Manage.* 45, 1759 – 1769.
- 466 [28] Hunt, L., Kuchar, L., Swanton, C., 1998. Estimation of solar radiation for use in crop mod-  
467 elling. *Agric. For. Meteorol.* 91, 293 – 300.
- 468 [29] Liu, D., Scott, B., 2001. Estimation of solar radiation in Australia from rainfall and temper-  
469 ature observations. *Agric. For. Meteorol.* 106 (1), 41 – 59.
- 470 [30] McCaskill, M., 1990. An efficient method for generation of full climatological records from  
471 daily rainfall. *Aust. J. Agric. Res.* Aust. J. Agric. Res., 595–602.
- 472 [31] McCaskill, M., 1990. Prediction of solar radiation from rainday information using region-  
473 ally stable coefficients. *Agric. For. Meteorol.* 51, 247–255.
- 474 [32] Weiss, A., Hays, C. J., 2004. Simulation of daily solar irradiance. *Agric. For. Meteorol.* 123,  
475 187 – 199.
- 476 [33] Meza, F., Varas, E., 2000. Estimation of mean monthly solar global radiation as a function  
477 of temperature. *Agric. For. Meteorol.* 100, 231 – 241.
- 478 [34] Prieto, J., Martínez-García, J., García, D., 2009. Correlation between global solar irradiation  
479 and air temperature in Asturias, Spain. *Sol. Energy* 83 (7), 1076 – 1085.
- 480 [35] Abraha, M., Savage, M., 2008. Comparison of estimates of daily solar radiation from air  
481 temperature range for application in crop simulations. *Agric. For. Meteorol.* 148 (3), 401 –  
482 416.
- 483 [36] Donatelli, M., Campbell, G., 1998. A simple model to estimate global solar radiation. In:  
484 Proc. ESA Cong., 5th, Nitra, Slovak Republic, 28 June- 2 July, 1998. The Slovak Agriculture  
485 University, 133–134.

- 486 [37] Goodin, D. G., Hutchinson, J. M. S., Vanderlip, R. L., Knapp, M. C., 1999. Estimating solar  
487 irradiance for crop modeling using daily air temperature data. *Agron. J.* 91 (5), 845–851.
- 488 [38] Weiss, A., Hays, C. J., Hu, Q., Easterling, W. E., 2001. Incorporating bias error in calculating  
489 solar irradiance: Implications for crop yield simulations. *Agron. J.* 93 (6), 1321–1326.
- 490 [39] Almorox, J., Hontoria, C., Benito, M., 2011. Models for obtaining daily global solar radi-  
491 ation with measured air temperature data in Madrid (Spain). *Appl. Energ.* 88 (5), 1703 –  
492 1709.
- 493 [40] Mavromatis, T., Jagtap, S. S., 2005. Estimating solar radiation for crop modeling using tem-  
494 perature data from urban and rural stations. *Climate Res.* 29 (3), 233–243.
- 495 [41] Thornton, P. E., Running, S. W., 1999. An improved algorithm for estimating incident daily  
496 solar radiation from measurements of temperature, humidity, and precipitation. *Agric. For.*  
497 *Meteorol.* 93 (4), 211 – 228.
- 498 [42] Winslow, J. C., Hunt, E. R., Piper, S. C., 2001. A globally applicable model of daily solar  
499 irradiance estimated from air temperature and precipitation data. *Ecol. Model.* 143 (3), 227  
500 – 243.
- 501 [43] Korpela, M., Mäkinen, H., Nöjd, P., Hollmén, J., Sulkava, M., Jun. 2010. Automatic detec-  
502 tion of onset and cessation of tree stem radius increase using dendrometer data. *Neuro-*  
503 *computing* 73, 2039–2046.
- 504 [44] Sos Rioja  
505 URL <http://www.larioja.org/npRioja/default/defaultpage.jsp?idtab=441001>
- 506 [45] Siar  
507 URL <http://ias1.larioja.org/estaciones/estaciones/siar/portada/index.jsp>
- 508 [46] Lawrence, S., Giles, C. L., Tsoi, A. C., 1996. What size neural network gives optimal gen-  
509 eralization? Convergence properties of backpropagation. Technical Report UMIACS-TR-  
510 96-22 and CS-TR-3617. Institute for Advanced Computer Studies. University of Maryland  
511 College Park, MD 20742, 1–35.
- 512 [47] Crawley, M. J., 2005. *Statistics: an introduction using R*. John Wiley.
- 513 [48] Mora, J., Mora-López, L., 2010. Comparing distributions with bootstrap techniques: An  
514 application to global solar radiation. *Math. Comput. Simulat.* 81 (4), 811 – 819.
- 515 [49] Varadhan, R., 2012. BB: Solving and optimizing large-scale nonlinear systems, r package  
516 version 2012.3-1 (2012).  
517 URL [URL <http://cran.r-project.org/web/packages/BB/BB.pdf>](http://cran.r-project.org/web/packages/BB/BB.pdf)
- 518 [50] Broyden, C. G., 1970. The convergence of a class of double-rank minimization algorithms.  
519 General considerations. *IMA J. Appl. Math.* 6 (1), 76–90.
- 520 [51] Nielsen, H., Mortensen, S., 2007. ucminf: General-purpose unconstrained non-linear opti-  
521 mization.  
522 URL <http://CRAN.R-project.org/package=ucminf>
- 523 [52] Willmott, C. J., Matsuura, K., 2005. Advantages of the mean absolute error (MAE) over  
524 the root mean square error (RMSE) in assessing average model performance. *Climate Res.*  
525 30 (1), 79–82.

- 526 [53] Moreno, A., Gilabert, M., Martínez, B., 2011. Mapping daily global solar irradiation over  
527 Spain: A comparative study of selected approaches. *Sol. Energy* 85 (9), 2072 – 2084.
- 528 [54] R Development Core Team, 2012. R: A language and environment for statistical computing.  
529 R Foundation for Statistical Computing, Vienna, Austria, ISBN 3-900051-07-0.  
530 URL <http://www.R-project.org>
- 531 [55] Pebesma, E. J., 2004. Multivariable geostatistics in s: the gstat package. *Comput. Geosci.*  
532 30, 683–691.
- 533 [56] Pebesma, E. J., Bivand, R. S., November 2005. Classes and methods for spatial data in R. *R*  
534 *News* 5 (2), 9–13.  
535 URL <http://CRAN.R-project.org/doc/Rnews/>
- 536 [57] Nash, J. C., Varadhan, R., 2012. optimx: A replacement and extension of the optim() func-  
537 tion.  
538 URL <http://cran.r-project.org/web/packages/optimx/index.html>
- 539 [58] Perpiñán, O., 2012. solaR: Solar radiation and photovoltaic systems with R. *J. Stat. Softw.*  
540 50 (9), 1–32.  
541 URL <http://www.jstatsoft.org/v50/i09/>
- 542 [59] Hijmans, R. J., van Etten, J., 2012. raster: Geographic analysis and modeling with raster  
543 data.  
544 URL <http://cran.r-project.org/web/packages/raster/>
- 545 [60] Perpiñán, O., Hijmans, R., 2012. rasterVis: Visualization methods for the raster package. R  
546 package version 0.10-9.  
547 URL <http://CRAN.R-project.org/package=rasterVis>
- 548 [61] Cleveland, W., 1979. Robust locally weighted regression and smoothing scatterplots. *Journal*  
549 *of the American Statistical Association* 74 (368): 829–836.
- 550 [62] Gueymard, C., Jindra, P., Estrada-Cajigal, V., 1995. A critical look at recent interpretations  
551 of the Angstrom approach and its future in global solar radiation prediction. *Sol. Energy*  
552 54 (5), 357 – 363.
- 553 [63] Antonanzas-Torres, F., Cañizares, F., Perpiñán, O., 2013. Comparative assessment of global  
554 irradiation from a satellite estimate model (CM SAF) and on-ground measurements (SIAR):  
555 a Spanish case study. *Renew. Sust. Energ. Rev.* 21 248-261.

Model no.	Equation	Parameters	Authors
1	$R_s = a\sqrt{\Delta T}R_a$	a	[9]
2	$R_s = a \left(1 + 2.7 \cdot 10^{-5} \cdot h\right) \sqrt{\Delta T}R_a$	a	[26]

*Continued on next page*

Model no.	Equation	Parameters	Authors
3	$R_s = (a\sqrt{\Delta T} + b) R_a$	a, b	[27]
4	$R_s = (a \cdot \ln(\Delta T) + b) R_a$	a, b	[27]
5	$R_s = a\sqrt{\Delta T} R_a + b$	a, b	[28]
6	$R_s = a\sqrt{\Delta T} R_a + b \cdot T_{max} + c \cdot P + d \cdot P^2 + e$	a, b, c, d, e	[28]
7	$R_s = a \cdot R_a \cdot \Delta T^b (1 + c \cdot P + d \cdot P^2)$	a, b, c, d	[10]
8	$R_s = a(1 - \exp(-b \cdot \Delta T^c)) R_a$	a, b, c	[8]
9	$R_s = a \cdot R_a (1 - \exp(-b\sqrt{\Delta T} - c \cdot \Delta T - d \cdot \Delta T^2))$	a, b, c, d	[28]
10	$R_s = a \left(1 - \exp\left(-b \frac{\Delta T^c}{R_a}\right)\right) R_a$	a, b, c	[37]
11	$R_s = a \left(1 - \exp\left(-b \frac{\Delta T^c}{R_{a,i-30}}\right)\right) R_a$	a, b, c	[38]
12	$R_s = 0.7 \left(1 - \exp(-b \cdot \Delta T^{2.4})\right) R_a$	b	[33]
13	$R_s = 0.75 \left(1 - \exp(-b \cdot \Delta T^2)\right) R_a$	b	[19]

*Continued on next page*

Model no.	Equation	Parameters	Authors
14	$R_s = 0.75 \left( 1 - \exp \left( -b \cdot \frac{\Delta T^2}{\Delta T_m} \right) \right) R_a$	b	[19]
15	$R_s = \left( a \cdot \Delta T^b \right) R_a$	a, b	[22]
16	$R_s = a + b \cdot \cos(\theta) + c \cdot \sin(\theta) + d \cdot \cos(2\theta) + e \cdot \sin(2\theta) + f \cdot M_{j-1} + g \cdot M_j + h \cdot M_{j+1}$	a, b, c, d, e, f, g, h	[30]
17	$R_s = a \cdot R_a + b \cdot M_{j-1} + c \cdot M_j + d \cdot M_{j+1}$	a, b, c, d	[31]
18	$R_s = R_a \cdot a (1 - \exp(-b \cdot \Delta T^c)) \cdot (1 + d \cdot M_{j-1} + e \cdot M_j + f \cdot M_{j+1}) + g$	a, b, c, d, e, f, g	[29]
19	$R_s = R_a \cdot a (1 - \exp(-b \cdot \Delta T^c)) + d \cdot M_{j-1} + e \cdot M_j + f \cdot M_{j+1} + g$	a, b, c, d, e, f, g	[29]
20	$R_s = a \left( 1 - \exp \left( -b \frac{\Delta T^c}{\Delta T_m} \right) \right) R_a$	a, b, c	[36]
21	$R_s = 0.75 \left( 1 - \exp \left( -b \cdot \Delta T^2 \cdot f(T_{avg}) \right) \right)$ $f(T_{avg}) = 0.017 \exp(\exp(-0.053 \cdot T_{avg} \cdot \Delta T))$	b	[36]

*Continued on next page*



Model no.	Equation	Parameters	Authors
22	$R_s = a \cdot R_a \cdot \Delta T^b (1 - \exp(-c \cdot p_{sat}[T_{max}]))^d$	a, b, c, d	[39]
23	$R_s = R_a \cdot a (1 - \exp(-b \cdot \Delta T^c)) \cdot (1 + d \cdot M_{j-1} + e \cdot M_j + f \cdot M_{j+1} + g \cdot \Delta T_{j+1} + h \cdot \Delta T_{j-1}) + l$	a, b, c, d, e, f, g, h, l	Proposed model
24	$R_s = R_a \cdot a (1 - \exp(-b \cdot \Delta T^c)) \cdot (1 + d \cdot M_{j-1} + e \cdot M_j + f \cdot M_{j+1} + g \cdot \Delta T_{j+1} + h \cdot \Delta T_{j-1} + l \cdot W_j + m \cdot H_j) + n$	a, b, c, d, e, f, g, h, l, m, n	Proposed model

Table 1: Summary of the twenty-three parametric models studied.  $\Delta T$  is the difference between  $T_{max}$  and  $T_{min}$ .  $R_{a,i-30}$  is the extraterrestrial irradiation on day  $i-30$ ,  $h$  is the elevation above sea level,  $T_{avg}$  is the daily average air temperature,  $\Delta T_m$  is the monthly average of  $\Delta T$  and  $p_{sat}[T_{max}]$  is the vapor saturation pressure at  $T_{max}$

#	Name	Net.	Lat.(°)	Long.(°)	Alt.	$\overline{\Delta T_c}$	$\overline{\Delta T_t}$	$P_c$	$P_t$	$\overline{R_{s,c}}$	$\overline{R_{s,t}}$
1	Agoncillo	SIAR	42.46	-2.29	342	12.3	12.6	484	318	14.7	15.3
2	Aldeanueva	SIAR	42.22	-1.90	390	11.1	11.4	405	327	15.4	15.4
3	Alfaro	SIAR	42.15	-1.77	315	12.5	12.9	335	364	15.3	15.2
4	Casalarreina	SIAR	42.53	-2.89	510	11.8	12.4	486	341	14.2	14.2
5	Cervera	SIAR	42.00	-1.89	495	13.9	14.3	356	331	15.2	15.0
6	Foncea	SIAR	42.60	-3.03	669	10.1	10.5	647	422	14.8	14.7
7	Leiva	SIAR	42.49	-3.04	595	11.4	11.5	499	379	14.5	14.4
8	Rincon	SIAR	42.25	-1.85	277	12.3	12.7	393	348	15.3	15.5
9	Urunuela	SIAR	42.46	-2.71	465	11.4	12.4	476	345	14.1	14.2
10	Aguilar	SOS	41.96	-1.96	752	9.3	9.7	463	236	14.5	14.7
11	Calahorra	SOS	42.29	-1.99	350	11.1	11.3	305	250	13.3	13.4
12	Ezcaray	SOS	42.33	-3.00	1000	10.3	10.7	538	381	13.6	13.6
13	Logroño	SOS	42.45	-2.74	408	10.1	10.3	423	212	14.3	14.3
14	Moncalvillo	SOS	42.32	-2.61	1495	7.8	7.7	567	429	12.0	11.9
15	San Roman	SOS	42.23	-2.45	1094	8.2	8.2	323	332	13.9	14.2

#	Name	Net.	Lat.(°)	Long.(°)	Alt.	$\overline{\Delta T_c}$	$\overline{\Delta T_t}$	$P_c$	$P_t$	$\overline{R_{s,c}}$	$\overline{R_{s,t}}$
16	Ventrosa	SOS	42.17	-2.84	1565	7.4	7.7	447	412	12.2	12.1
17	Villoslada	SOS	42.12	-2.66	1235	9.7	9.9	499	325	12.6	12.4

Table 2: Summary of the seventeen meteorological stations.  $\overline{\Delta T_c}$  and  $\overline{\Delta T_t}$  are the average  $\Delta T$  of the *calibration* and *testing* datasets, respectively.  $P_c$  is the yearly average rainfall in mm for the *calibration* dataset and  $P_t$  is the yearly rainfall for the *testing* dataset.  $\overline{R_{s,c}}$  and  $\overline{R_{s,t}}$  are the daily average  $R_s$  for the *calibration* and *testing* datasets, respectively

$v$	$P_i$	$P_{i+1}$	$P_{i-1}$	$M_i$	$M_{i+1}$	$M_{i-1}$	$\Delta T_i$	$\Delta T_{i+1}$	$\Delta T_{i-1}$	$\Delta T_{i+2}$	$\Delta T_{i-2}$
$R^2$	0.056	0.012	0.016	0.153	0.068	0.059	0.533	0.359	0.340	0.301	0.172
$v$	$\Delta T_{i+3}$	$\Delta T_{i-3}$	$W_i$	$W_{i+1}$	$W_{i-1}$	$H_i$	$H_{i+1}$	$H_{i-1}$	$H_{i+2}$	$H_{i-2}$	
$R^2$	0.206	0.167	0.089	0.076	0.071	0.465	0.344	0.251	0.251	0.199	

Table 3: Summary of variable importance results related to each variable  $v$

Model	1	2	3	4	5	6	7	8	9	10	11	12
$\overline{MAE}_{val}$	2.814	2.809	2.699	2.679	2.797	2.768	2.534	2.617	2.613	2.791	4.426	2.791
$\overline{R}_{MAE, val}$	0.436	0.415	0.426	0.425	0.411	0.430	0.420	0.420	0.422	0.423	0.761	0.527
$\overline{RMSE}_{val}$	3.572	3.560	3.475	3.448	3.541	3.488	3.409	3.294	3.398	3.584	5.873	3.825
$\overline{R}_{RMSE, val}$	0.559	0.545	0.601	0.569	0.549	0.539	0.577	0.605	0.593	0.579	0.996	0.745
Model	13	14	15	16	17	18	19	20	21	22	23	24
$\overline{MAE}_{val}$	2.804	2.751	2.719	6.273	3.366	2.317	2.336	2.678	2.728	2.723	2.247	2.195
$\overline{R}_{MAE, val}$	0.491	0.488	0.444	0.764	0.498	0.387	0.385	0.445	0.498	0.432	0.360	0.261
$\overline{RMSE}_{val}$	3.798	3.708	3.485	7.377	4.256	3.023	3.081	3.457	3.693	3.504	2.995	2.879
$\overline{R}_{RMSE, val}$	0.715	0.691	0.583	0.802	0.649	0.548	0.538	0.606	0.694	0.576	0.543	0.361

Table 4: Summary of statistics in MJ/m<sup>2</sup>day

Mod. 18	1	2	3	4	5	6	7	8	9	10	11	12	13	14	15	16	17
$p - value$	0.9	0.9	0.9	0.6	0.9	0.8	0.8	0.9	0.0	0.9	0.6	0.9	0.9	0.7	0.9	0.6	0.9
Mod. 23	1	2	3	4	5	6	7	8	9	10	11	12	13	14	15	16	17
$p - value$	0.9	0.9	0.9	0.9	0.9	0.7	0.4	0.9	0.0	0.9	0.7	0.6	0.9	0.7	0.3	0.6	0.9

Table 5: Summary of  $p - values$  of  $t - test$  in the  $MAE_{val}$  of model 24 against model 18 and model 23 ( $p - values$  greater than 0.05 imply statistically significant lower  $MAE_{val}$  in model 24)

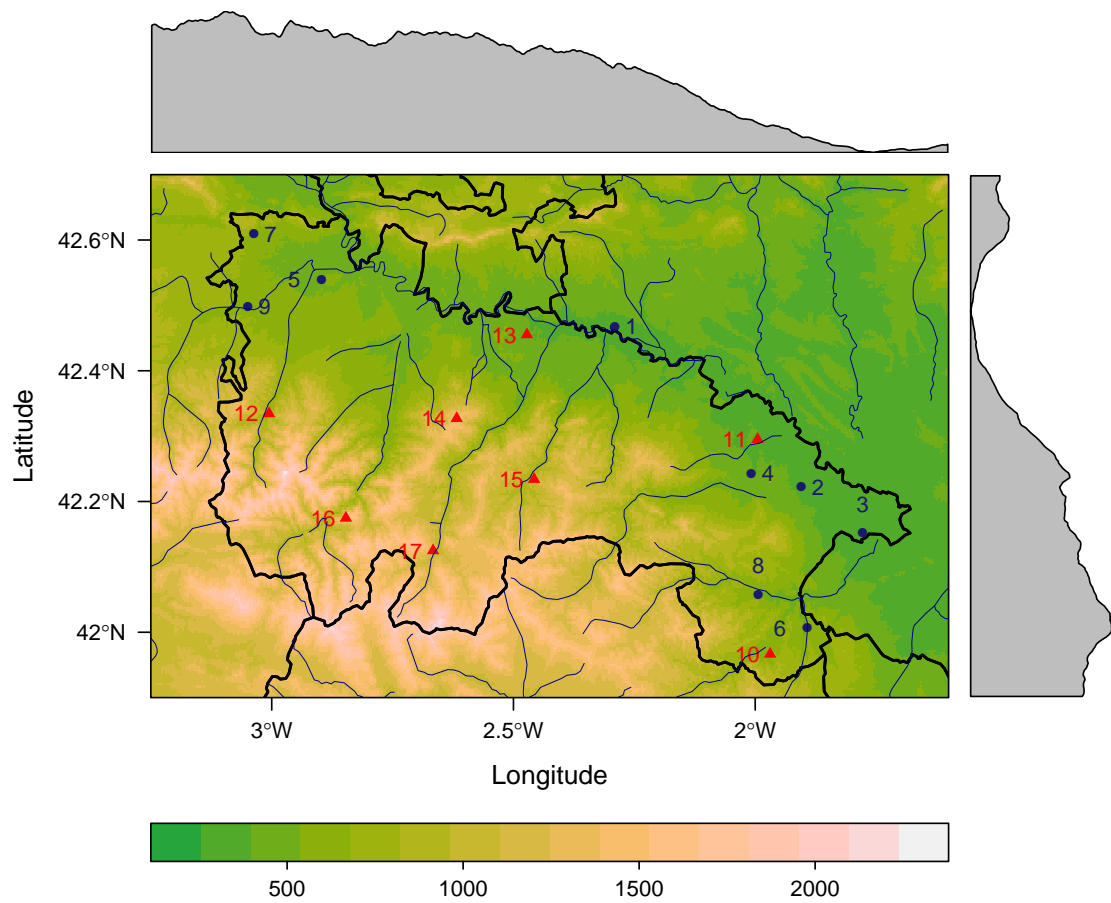


Figure 1: Location of the meteorological stations selected in the region of La Rioja. The color band represents elevation (m). SIAR stations are shown by blue circles and SOS Rioja stations by red triangles

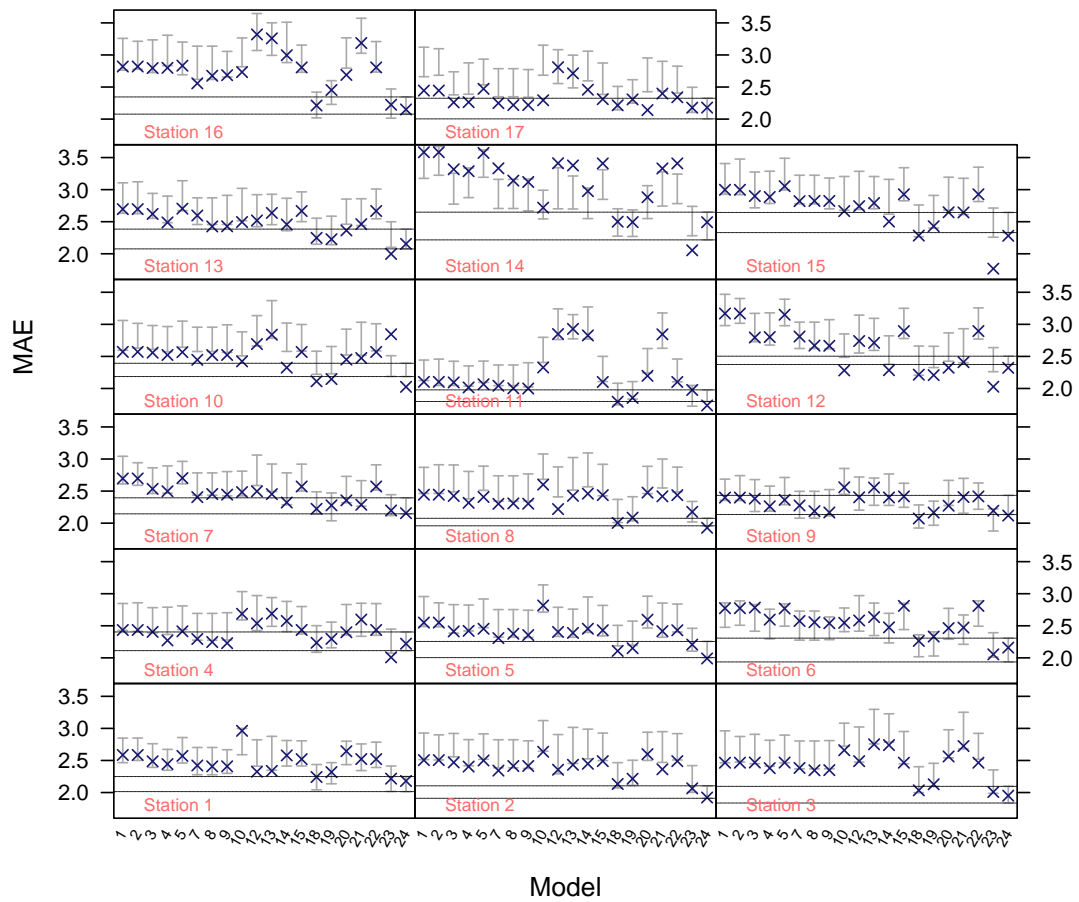


Figure 2: Confidence intervals (95% C.I.,  $n=100$ ) of  $MAE_{val}$  (grey vertical lines) and  $MAE_{tes}$  (blue crosses) ( $MJ/m^2/day$ ). Note that some of the values of models 11, 16 and 17 lie outside the range of the figure

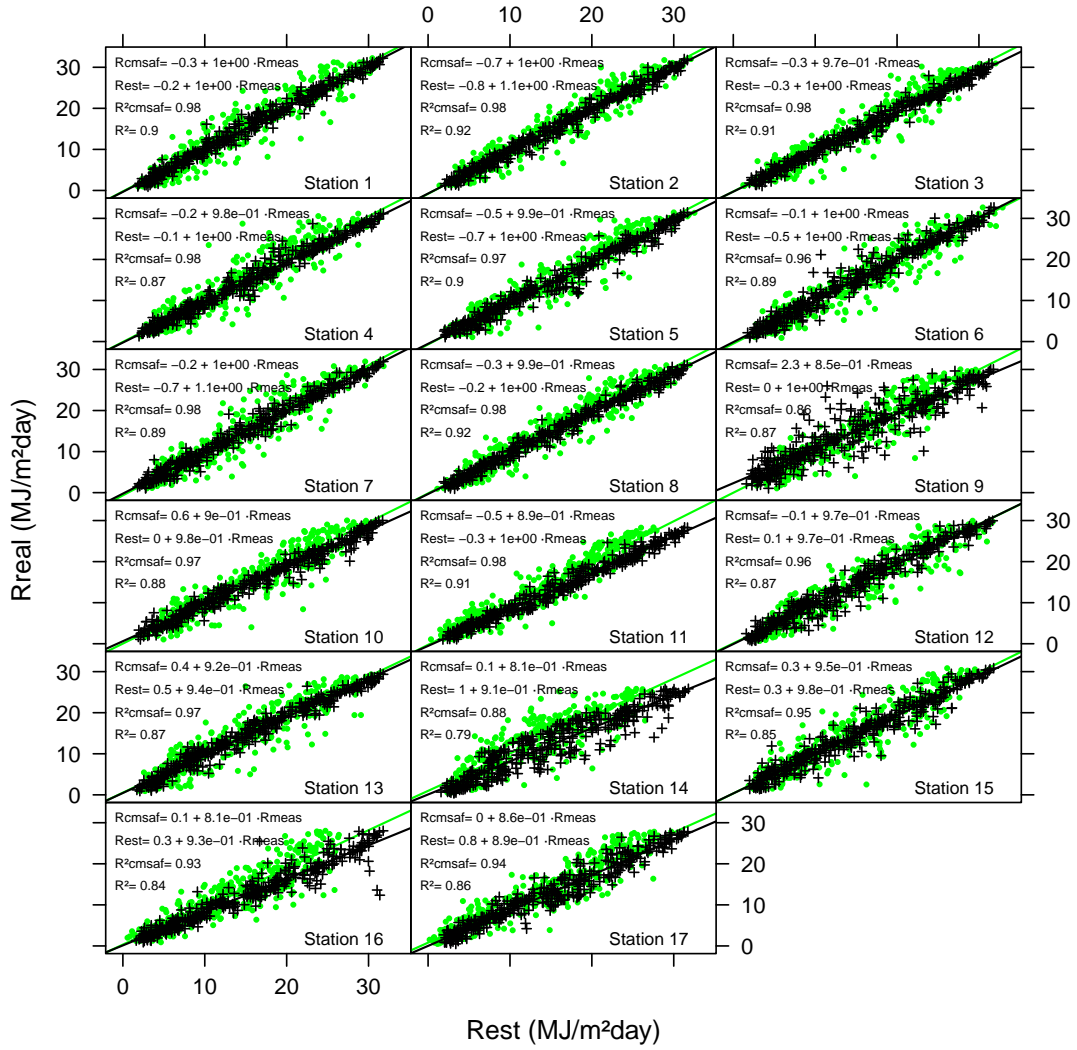


Figure 3: Correlation between  $R_{s,meas}$  (MJ/m<sup>2</sup>day) and  $R_{s,est}$  of the model proposed (model 24) with green points and  $R_{s,cmsaf}$  with black crosses within the *testing* time series at all seventeen stations

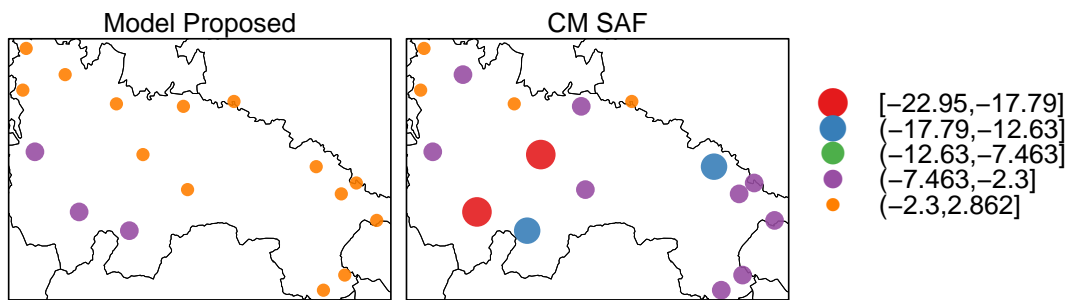


Figure 4: Annual relative difference (%) between  $R_{s,meas}$  and  $R_{s,est}$  for the model proposed (model 24) and CM SAF during the *testing* period (year 2011).

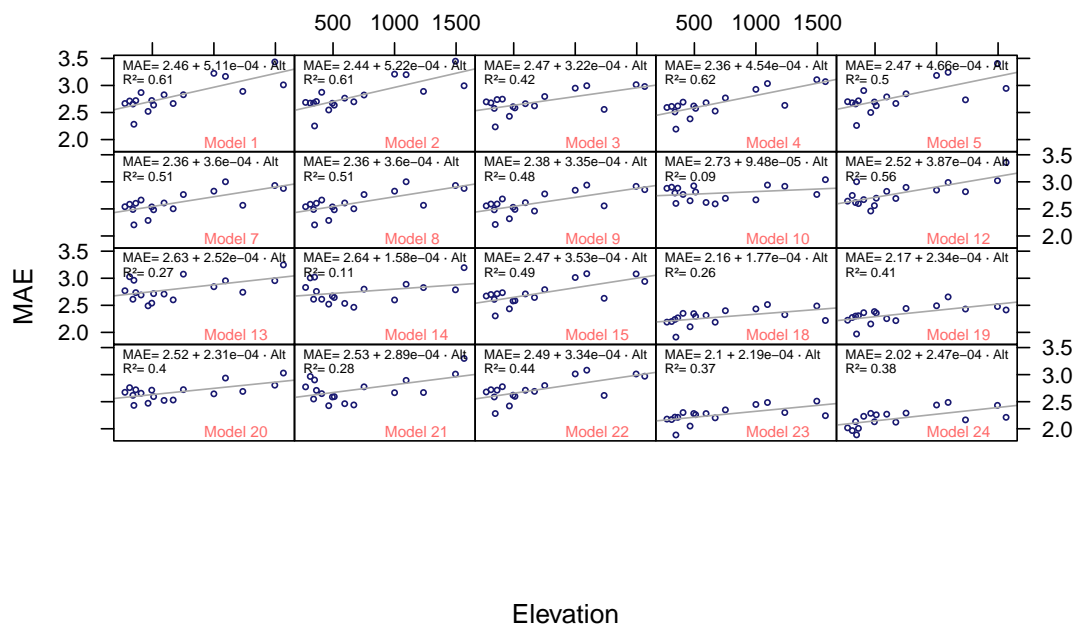
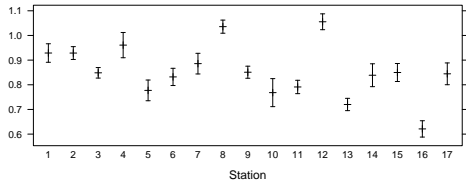
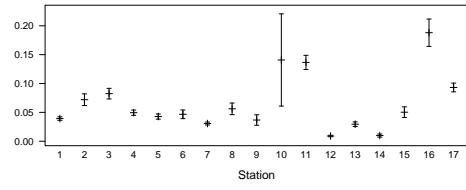


Figure 5: Relation between elevation (m) and median of the  $MAE_{val}$  ( $MJ/m^2/day$ ). Models 11, 16 and 17 are not shown due to their high  $MAE_{val}$

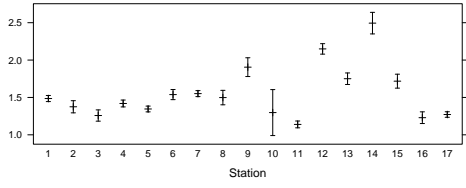




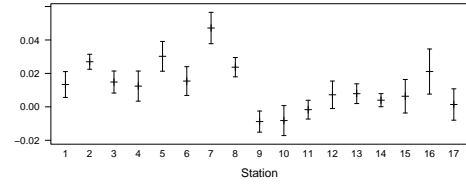
(a) Parameter a



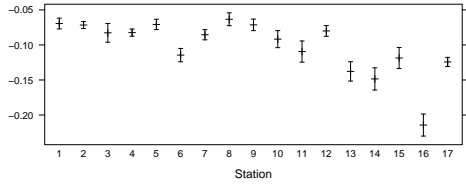
(b) Parameter b



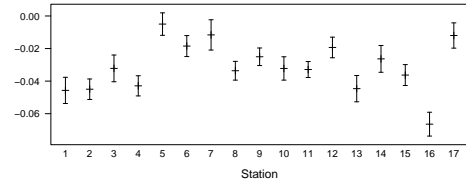
(c) Parameter c



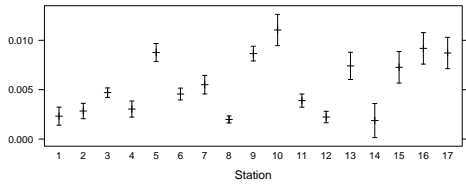
(d) Parameter d



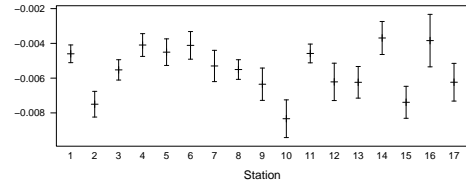
(e) Parameter e



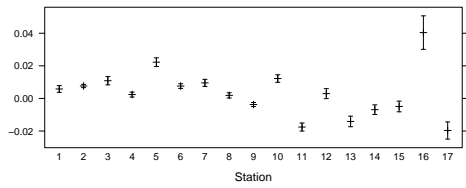
(f) Parameter f



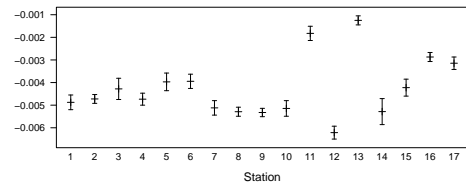
(g) Parameter g



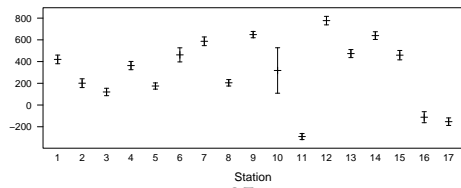
(h) Parameter h



(i) Parameter l



(j) Parameter m



(k) Parameter n

Figure 6: Confidence intervals (95% C.I., n=100) and median of the parameters of the proposed model (model 24)

Station	$MAE_{tes,24}$	$MAE_{tes,CMSAF}$	$RMSE_{tes,24}$	$RMSE_{tes,CMSAF}$
1	2.18	0.91	2.85	1.20
2	1.92	0.86	2.46	1.17
3	1.95	1.05	2.55	1.33
4	2.22	1.09	3.00	1.43
5	1.99	1.12	2.65	1.60
6	2.16	1.13	2.83	1.67
7	2.16	0.95	2.89	1.29
8	1.93	0.93	2.45	1.19
9	2.12	2.27	2.79	3.20
10	2.03	1.37	2.71	1.80
11	1.74	2.35	2.28	2.74
12	2.32	1.34	2.99	1.79
13	2.15	1.30	2.93	1.65
14	2.49	3.18	3.36	4.02
15	2.28	1.32	3.07	1.87
16	2.15	2.83	2.99	3.63
17	2.18	2.28	2.90	2.91

Table 6: Testing errors of model 24 and CM SAF (year 2011)

$a_{mean}$	$a_{sd}$	$b_{mean}$	$b_{sd}$
0.61	0.05	0.09	0.04

Table 7: Summary of CM SAF re-calibration as per Equation 9

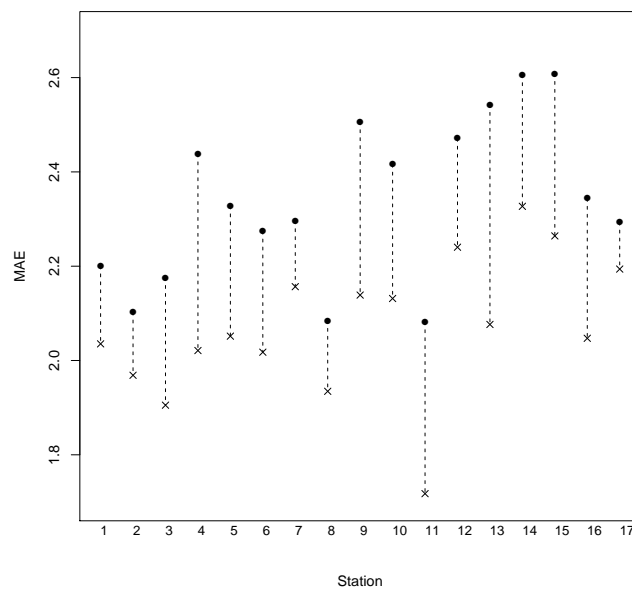


Figure 7: Average MAE (MJ/m<sup>2</sup>day) of the proposed model (model 24) for rainy days (black dots) and non-rainy days (black crosses)